

# Fluidized Bed Selective Oxidation-Sulfation Roasting of Nickel Sulfide Concentrate: Part I. Oxidation Roasting

DAWEI YU, TORSTEIN A. UTIGARD, and MANSOOR BARATI

Two-stage oxidation-sulfation roasting of nickel sulfide concentrate in fluidized bed was investigated to generate water-soluble metal sulfates as an alternative process to smelting of the sulfide concentrate for the recovery of valuable metals. The first stage, *i.e.*, oxidation roasting, was employed to preferentially oxidize the iron before performing sulfation roasting. A batch fluidized bed roaster was constructed for roasting tests. Roasting products from various roasting temperatures and different roasting times were analyzed by SEM/EDS, EPMA, XRD, and ICP-OES to investigate the oxidation roasting behavior of the nickel concentrate as a function of temperature and time.

DOI: 10.1007/s11663-013-9958-x

© The Minerals, Metals & Materials Society and ASM International 2013

## I. INTRODUCTION

SINCE the commercial production of nickel from the laterite deposits of New Caledonia in 1875, and later from the great sulfide deposits of the Sudbury district of Canada in 1885,<sup>[1]</sup> nickel extraction technologies have evolved into several routes. The production of nickel from saprolite (low-Fe laterite) is through reduction in rotary kilns followed by smelting in electric furnaces. The process is highly energy intensive in nature because laterites are not amenable to concentration by physical means and the feed to a laterite smelter contains 35 pct to 47 pct water in the form of free moisture and crystalline water.<sup>[2]</sup> Limonite and smectite (high-Fe laterite) are treated by high-pressure acid leaching process (HPAL process).<sup>[3]</sup> Limonite-type laterite is also treated with the Caron process, which comprises pyrometallurgical reduction followed by leaching with aqueous  $\text{NH}_3 + \text{CO}_2 + \text{O}_2$  solution.<sup>[3]</sup> On the other hand, nickel sulfide minerals are upgraded through efficient and cost-effective milling and flotation,<sup>[4]</sup> with a concentration factor of about 20.<sup>[5]</sup> In contrast to laterite smelting, pyrometallurgical processing of nickel sulfide minerals is relatively energy efficient, mainly due to the utilization of energy from the exothermic oxidation of sulfides, as well as the ease of beneficiation of the sulfide ores. As a result, the exploitation of sulfide ores for nickel production has historically exceeded that of oxide ores, despite the geographical predominance of the later.<sup>[1]</sup>

There are two routes for the processing of the nickel sulfide concentrate, namely flash smelting and electric

furnace smelting, both of which produce large quantities of  $\text{SO}_2$ . As a way of mitigating  $\text{SO}_2$ , its fixation mostly in the form of sulfuric acid ( $\text{H}_2\text{SO}_4$ ) is an integral part of the processing routes. Sulfuric acid plants require an optimum  $\text{SO}_2$  concentration in the offgas to be between 10 pct and 12 pct.<sup>[6]</sup> Generally, the flash furnace and the fluidized bed roaster produce a continuous offgas stream with suitable  $\text{SO}_2$  concentration, whereas the offgas released from the electric furnaces and Pierce-Smith converters contains less than favorable  $\text{SO}_2$  concentrations. The converter emits  $\text{SO}_2$  into the environment during charging and skimming, which produces a discontinuous flow of  $\text{SO}_2$  to the  $\text{H}_2\text{SO}_4$  plant.<sup>[6]</sup>

In an attempt to lower the environmental footprint of nickel processing, and as an alternative process to treat nickel sulfide concentrate, a two-stage oxidation-sulfation roasting process followed by leaching was proposed and investigated. Sulfation roasting to treat nickeliferous sulfide ores or low grade concentrates was investigated in the period from 1960s to 1990s.<sup>[7-16]</sup> In general, the sulfation roasting process suffers from the drawbacks of slow kinetics and low recovery of non-ferrous metals, Ni in particular, due to the formation of nickel ferrite ( $\text{NiFe}_2\text{O}_4$ ) at high temperatures [ $>973 \text{ K}$  ( $700 \text{ }^\circ\text{C}$ )], which is resistant to sulfation. These studies in general lack detailed investigation on the kinetics and mechanisms of the sulfation roasting of nickel sulfide concentrate, which could advantageously be used to address the above issues. In addition, with more stringent environmental regulations, a renewed interest in further studying the prospects of the proposed technology is warranted. The scope of study includes two-stage oxidation-sulfation roasting, leaching of the calcines, and further recovery of Ni from leached residue through high temperature reduction. This two-part series focuses on the optimization of the roasting steps with the aim of maximizing recovery of valuable metals into the leach solution. A third article<sup>[17]</sup> discusses the recovery of Ni from the leach residue. This article presents an overview of the methods and findings from fluidized bed oxidation roasting of nickel concentrates.

---

DAWEI YU, Ph.D. Candidate, is with the Department of Materials Science and Engineering, University of Toronto, 184 College Street, Suite 140, Toronto, ON M5S3E4, Canada. Contact e-mail: dawei.yu@mail.utoronto.ca TORSTEIN A. UTIGARD, formerly Professor with the Department of Materials Science and Engineering, University of Toronto, is now deceased. MANSOOR BARATI, Associate Professor, is with the Department of Materials Science and Engineering, University of Toronto.

Manuscript submitted April 24, 2013.

Article published online October 8, 2013.

**Table I. Chemical Composition of the Raglan Concentrate**

Constituents	Ni	Fe	Cu	Co	S	MgO	Al <sub>2</sub> O <sub>3</sub>	SiO <sub>2</sub>	Total
Weight pct	17.9	30.8	4.54	0.36	27.6	5.43	0.76	8.69	96.1

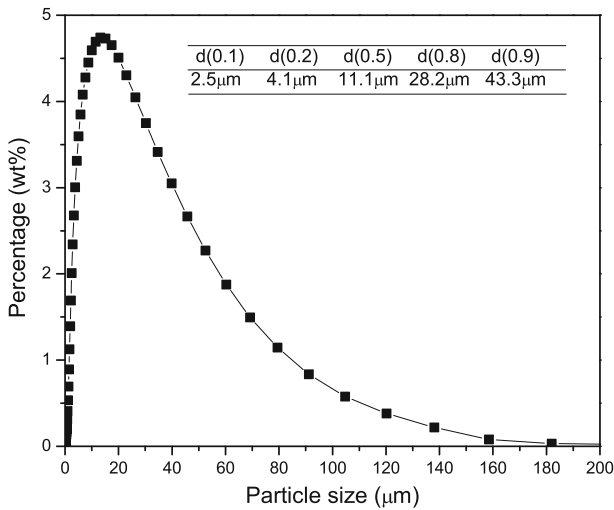


Fig. 1—Particle size distribution of the Raglan concentrate.

The results from the investigation of the second stage, *i.e.*, sulfation roasting, are presented in the second article in this series.<sup>[18]</sup>

## II. MATERIALS AND METHODS

### A. Materials

Raglan concentrate from Xstrata Nickel’s smelter in Sudbury, Canada was used in the experiments. The concentrate consists of pentlandite (Fe,Ni)<sub>9</sub>S<sub>8</sub>, chalcopyrite CuFeS<sub>2</sub>, pyrrhotite Fe<sub>1-x</sub>S, as well as a small amount of siliceous gangue. The chemical composition of a representative sample is provided in Table I. The particle size distribution of the material was obtained using a Laser Particle Size Analyzer (Hydro 2000S, Malvern Instruments) with the results shown in Figure 1. Sieve analysis shows 99.4 pct passing 140 mesh (106 μm), 93.3 pct passing 200 mesh (74 μm), and 76.7 pct passing 400 mesh (37 μm).

### B. Experimental

Compared to oxidation roasting, sulfation roasting is characterized with slow kinetics and strong dependence on temperature.<sup>[19]</sup> In order to achieve the highest possible reaction rates and accurate temperature control during the roasting process, a fluidized bed technique was employed. A laboratory scale, batch-operated fluidized bed roaster was designed and constructed to allow conducting both oxidation and sulfation roasting experiments (Figure 2).

A clear quartz tube with inner diameter of 36 mm with an expanded top (66 mm inner diameter) was used

as the roasting reaction vessel. A porous frit was fused in the quartz tube acting as the gas distributor. The purpose of this design is to lower the velocity of the gas in the free board above the fluidized bed, thus alleviating the gas entrainment of solid particles. The quartz tube was mounted vertically in an electric furnace as shown in Figure 2. Its top opening was sealed with a brass cap to prevent the leakage of the offgas.

Roasting gas was fed from the bottom of the quartz tube. The offgas was cleaned in a gas scrubber (Buchi Scrubber B-414) to eliminate SO<sub>2</sub> before venting to the fume hood. A pneumatic dispenser was used to feed the concentrate to the sealed chamber using nitrogen as the carrier gas. During the roasting experiment, the temperature of the fluidized bed was measured using a K-type thermocouple. The pressure drop across the bed and the porous frit was measured by a pressure transducer (OMEGA PX302-015GV). The offgas was directed to a multi-channel gas analyzer (ABB EL3020) to measure its SO<sub>2</sub> and O<sub>2</sub> concentrations. These above data along with the feeding gas flowrate were recorded using a computer controlled data acquisition system (FLUKE Hydra Series II). In order to control the temperature of the fluidized bed and avoid overheating due to the exothermic roasting reactions, a stream of sand was injected to the reaction tube when necessary. Platinum catalyst was mounted beneath the porous frit only for sulfation roasting experiments. Once the fluidized bed roasting experiment was completed, the calcine was withdrawn from the quartz tube immediately. This was accomplished using a vacuum pump, which collects the calcine into a cyclone *via* a long ceramic tube. Quick collection of calcine out of the quartz tube was necessary to prevent decomposition of sulfates at high temperature.

The as-received concentrate could not fluidize in this fluidized bed roaster, as the gas was channeled through the bed. The concentrate was then fused together due to the immobility of the bed and highly exothermic reactions occurring in the bed. This is because the Raglan concentrate falls into Group C in the Geldart classification of powders.<sup>[20]</sup> The interparticle forces are greater than the force exerted by the up-flowing gas, resulting in the formation of channels instead of the concentrate being fluidized. To address this problem, sand, which is a type B material<sup>[20]</sup> was mixed with the concentrate. The particle size range of the sand should be preferably different from that of the concentrate to render the effective separation of the calcine from the sand after roasting simply by sieving. Results from trial runs show that the particle size range should be as close to that of the concentrate as possible to avoid the appreciable separation of the two materials during roasting. As a result, the particle size range of the sand was set to be 150 to 212 μm. In addition, the weight

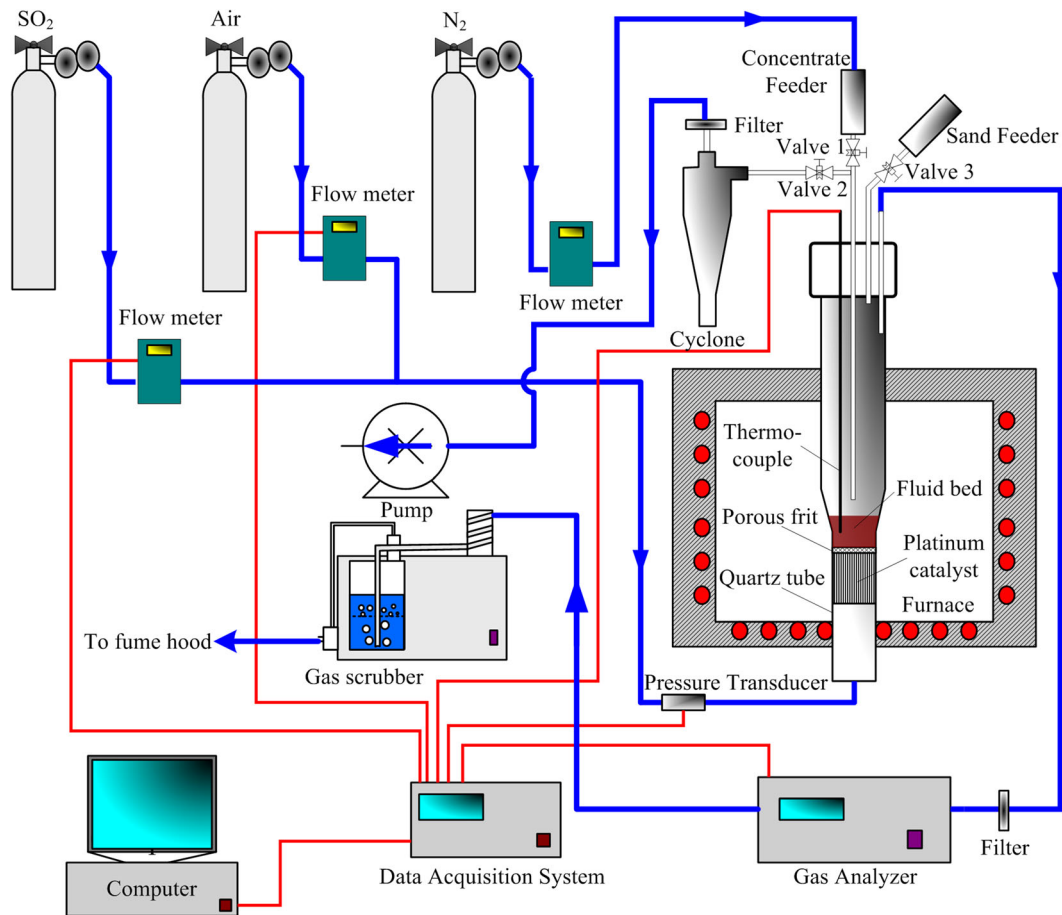


Fig. 2—Schematic of the batch-wise fluidized bed experimental setup.

ratio of sand to concentrate should be no less than approximately 4 to render a fluidized bed with enough mobility to avoid the occurrence of agglomeration due to local overheating. Based on these results, a batch of 5-gram Raglan concentrate was mixed with 20-gram sand with the particle size range between 150  $\mu\text{m}$  and 212  $\mu\text{m}$  before each roasting test. Separation between the resulting calcine and the sand was conducted simply by sieving based on the particle size range difference between these two materials.

Two series of oxidizing roasting tests were performed to study the effect of temperature and roasting time on the extent of oxidation and reaction products. Extra dried air was used as the feeding gas with a flowrate of 3 L/min. In the first series of tests, the temperature was varied in the range 923 K to 1048 K (650  $^{\circ}\text{C}$  to 775  $^{\circ}\text{C}$ ), while in the second set, the temperature was maintained at 1023 K (750  $^{\circ}\text{C}$ ) and the roasting times from 1 to 13 min were examined. The collected calcines were subjected to various analyses to evaluate the roasting performances.

### C. Analytical Methods

60 mg of the calcines were leached in 15 mL water at 363 K (90  $^{\circ}\text{C}$ ) for 30 min to evaluate the amount of water-soluble species formed during roasting. After

filtration, the leach residue (water-insoluble fraction) was dried and mixed with 5 g  $\text{Na}_2\text{O}_2$ . The mixture was then placed in a zirconium crucible and heated until a homogeneous melt was made. The fused sample was then cooled to room temperature and then dissolved in water. The solution formed was then neutralized by 18 wt pct HCl. Solutions from both leaching and  $\text{Na}_2\text{O}_2$  fusion were properly diluted and analyzed by inductively coupled plasma optical emission spectrometry (ICP-OES) for chemical composition determination and calculation of the percentages of the formation of water-soluble species based on Eq. [1], in which  $W_{(\text{Me, leach solution})}$  represents the weight of species Me in the leach solution and  $W_{(\text{Me, leach residue})}$  represents the weight of species Me in the residue calculated based on the ICP results.

$$\text{wt pct}_{(\text{Me, water-soluble})} = \frac{W_{(\text{Me, leach solution})}}{W_{(\text{Me, leach solution})} + W_{(\text{Me, leach residue})}} \times 100 \quad [1]$$

Samples were also analyzed by XRD using a Philips PW2273/20 diffractometer with  $\text{Cu K}_\alpha$  radiation. Calcines were further examined by scanning electron microscopy (SEM, JEOL JSM6610-Lv) equipped with EDS detector (Oxford/SSD) for characterization of

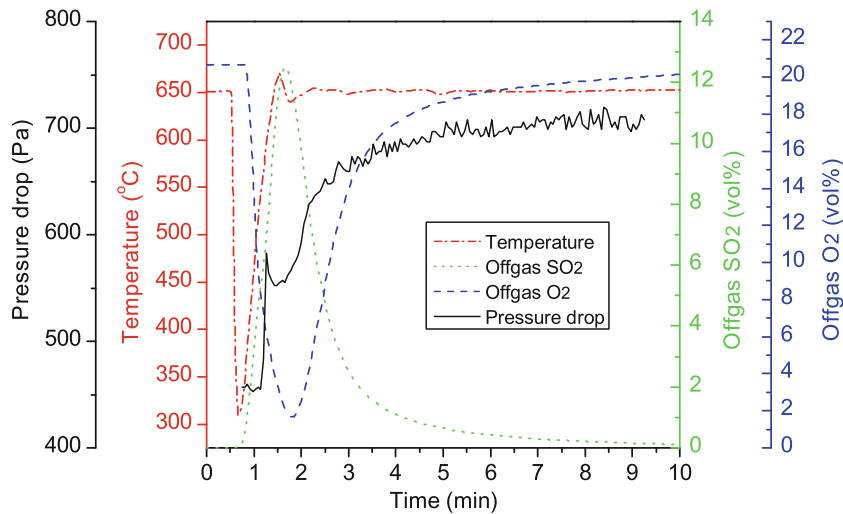


Fig. 3—Temperature, offgas SO<sub>2</sub> and O<sub>2</sub> concentrations, and pressure drop for roasting test at 923 K (650 °C).

morphology and mineralogy of the phases formed. Elemental analyses were acquired on a Cameca SX50 electron probe microanalyzer (EPMA) equipped with 3 tunable wavelength dispersive spectrometers. Operating conditions were 40° takeoff angle, and a beam energy of 20 keV. The beam current was 10 nA, and the beam diameter was 1 μm. Elements were acquired using analyzing crystals LiF for Fe K<sub>α</sub>, Ni K<sub>α</sub>, Co K<sub>α</sub>, PET for S K<sub>α</sub>, and PCI for O K<sub>α</sub>. The standards were cobaltite for Co K<sub>α</sub>, hematite for O K<sub>α</sub>, and pentlandite for S K<sub>α</sub>, Fe K<sub>α</sub>, and Ni K<sub>α</sub>. The counting time was 20 s for Fe K<sub>α</sub>, Ni K<sub>α</sub>, S K<sub>α</sub>, 40 s for O K<sub>α</sub>, and 60 s for Co K<sub>α</sub>.

### III. RESULTS AND DISCUSSION

#### A. Effect of Roasting Temperature

The effect of oxidation roasting temperature was evaluated from 923 K to 1048 K (650 °C to 775 °C) with temperature increments of 25 K. During the start of testing, when the temperature of the fluidized bed tends to exceed the target temperature due to the exothermic roasting reactions, a stream of sand was applied to suppress the overheating. The temperature of the fluidized bed, offgas SO<sub>2</sub> and O<sub>2</sub> concentrations, and pressure drop across the porous frit and the fluidized bed were continuously measured, and have been plotted in Figure 3, for the roasting test at 923 K (650 °C) as an example. Similar plots were obtained for the roasting tests at other temperatures, exhibiting similar trends. As seen in Figure 3, at around 0.5 min, a rapid temperature drop and a corresponding Δ*P* increase were recorded, marking the start of feeding. The temperature recovered after reaching a low of around 573 K (300 °C). The temperature rise corresponds with a decline in O<sub>2</sub> and an increase in SO<sub>2</sub> indicating the progress of roasting reactions. The low in the O<sub>2</sub> curve is around 2 vol pct, corresponding to the SO<sub>2</sub> peak of around 13 vol pct. The volume of the free board, which is the volume above the

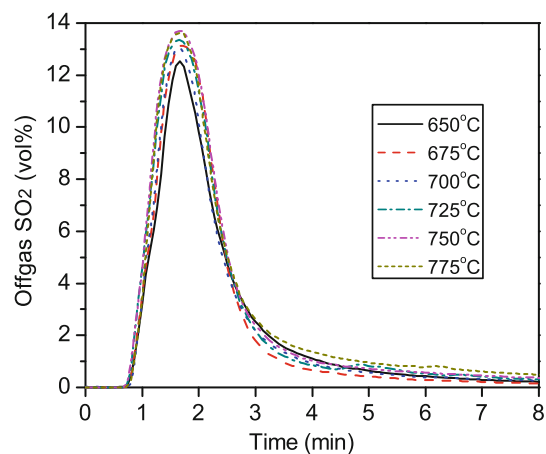


Fig. 4—Offgas SO<sub>2</sub> profiles for the fluidized bed roasting tests by air with roasting temperature variation.

fluidized bed in the quartz tube, is relatively large compared with that of the fluidized bed. Therefore, the offgas was held up and mixed to some extent in the free board during roasting before reaching the gas analyzer. As a result, the offgas O<sub>2</sub> concentration recorded in Figure 3 lags the actual value in the fluidized bed, as does the measured SO<sub>2</sub>. It is believed that the lowest O<sub>2</sub> concentration in the fluidized bed was lower than 2 vol pct. This indicates that at the time when the fluidized bed atmosphere was relatively starved of O<sub>2</sub>, the roasting reactions were so fast that the O<sub>2</sub> in the roasting gas was consumed immediately when passing through the fluidized bed. The roasting rate controlling step would be the supply of O<sub>2</sub> to the fluidized bed, rather than the roasting reactions or the gaseous diffusion through the oxide layers. At later roasting stage when the partial pressure of O<sub>2</sub> in the fluidized bed was high, the gas diffusion through the oxide layers could dominate and control the overall roasting rate. The offgas SO<sub>2</sub> profiles for all roasting tests with temperature variation are plotted in Figure 4, which

exhibits the similarities in terms of the progress of roasting at different temperatures.

Calcine was collected when the roasting was close to completion for each temperature. This was performed by withdrawing the calcine with vacuum when the SO<sub>2</sub> concentration of the offgas dropped to below 0.3 vol pct, which is an indication of the near-completion of the roasting reactions. For oxidation roasting with air under normal roasting temperatures, the equilibrium phases are always oxides of various metals (Fe, Ni, Cu, Co) from a thermodynamic point of view. However, due to the limitations imposed by kinetics (*e.g.*, gas/solid diffusion, chemical reactions) and the varying local gas environment, sulfides and even sulfates could be present in the calcine products. XRD analysis was employed to evaluate the mineralogical composition of the calcine products. Their XRD patterns are presented in Figure 5. As can be seen, main compounds in these calcines are hematite (Fe<sub>2</sub>O<sub>3</sub>), trevorite (Ni<sub>x</sub>Fe<sub>3-x</sub>O<sub>4</sub>), nickel oxide (NiO), monosulfide solid solution (mss), and heazlewoodite (Ni<sub>3</sub>S<sub>2</sub>). There is no pentlandite, chalcopyrite, or pyrrhotite in the calcines. The content of hematite in the calcines does not change much with the increase of roasting temperature from 923 K to 1048 K (650 °C to 775 °C) since there is little difference with regards to its peak intensities. This is because iron sulfide species in the form of pyrrhotite, pentlandite, or chalcopyrite could be preferentially oxidized at lower temperatures.<sup>[21]</sup> Reaction [2] represents the complete oxidation of pyrrhotite below 923 K (650 °C). Figure 6 illustrates the morphology of partly oxidized pentlandite particles roasted at 923 K (650 °C). Iron sulfide was preferentially oxidized from pentlandite particles forming a hematite shell around the nickel-iron sulfide core (mss). The partial oxidation of pentlandite could be represented by Reaction [3]. Concentration profiles of a roasted pentlandite particle along the arrow in Figure 6 were measured by EPMA and are illustrated in Figure 7. Gradients of the Fe and Ni concentrations can be observed in the sulfide core. The center of the sulfide core has higher Fe concentration (7.5 at pct) and lower Ni concentration (41.5 at pct) than its edge (approximately 5 at pct Fe, 44 at pct Ni). These gradients indicate the outward diffusion of Fe to the surface of sulfide core where oxidation occurred. The hematite layer formed on the surface has approximately 2 at pct Ni, suggesting that a small portion of Ni was also oxidized along with the preferential oxidation of Fe species. Co was oxidized at a faster rate than Ni, resulting in the co-presence of Co in the hematite layer. At temperatures higher than 973 K (700 °C), the formation of trevorite and NiO is obvious as suggested by Figure 5. Monosulfide solid solution disappears at temperatures higher than 973 K (700 °C), which could be represented by Reaction [4], and heazlewoodite becomes the only sulfur-containing species. The amount of heazlewoodite in the calcines becomes smaller with the increase of roasting temperature, which can be seen by the decreasing intensities of the heazlewoodite peak at 31.2 deg with the increase of temperature. This suggests the oxidation of heazlewoodite forming NiO according to Reaction [5]. Based on the XRD analysis,

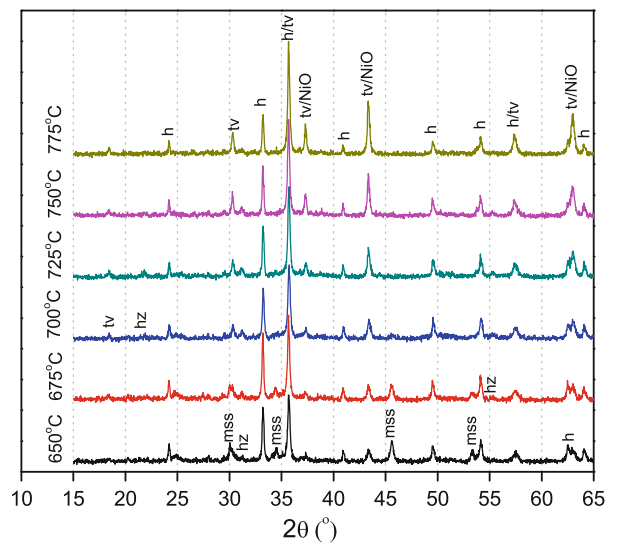


Fig. 5—XRD patterns for the fluidized bed roasting tests with temperature variation (tv: trevorite, NiFe<sub>2</sub>O<sub>4</sub>; mss: monosulfide solid solution, (Ni,Fe)<sub>1-x</sub>S; h: hematite, Fe<sub>2</sub>O<sub>3</sub>; NiO: nickel oxide; hz: heazlewoodite, Ni<sub>3</sub>S<sub>2</sub>).

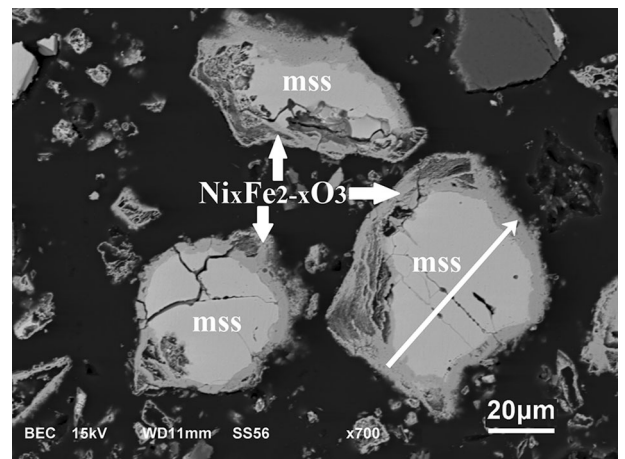
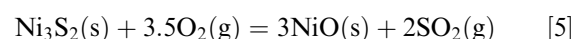
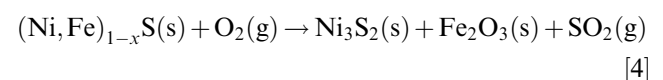
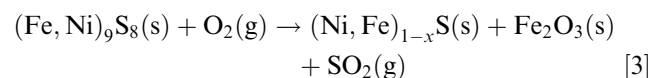
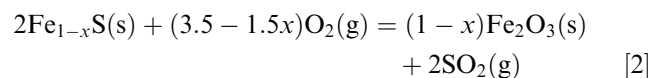


Fig. 6—Roasted pentlandite particles at 923 K (650 °C) with 3 L/min air (mss: monosulfide solid solution).

more species in the calcine appear in the form of oxides at higher temperatures and in the form of sulfides at low temperatures.



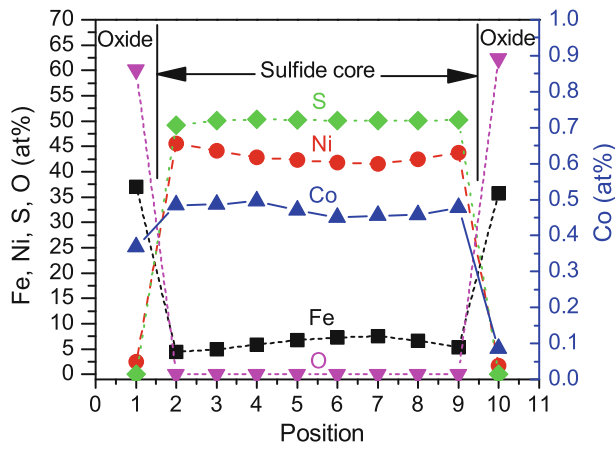


Fig. 7—Concentration profiles in a cross section of a roasted pentlandite particle [923 K (650 °C)] along the arrow in Fig. 6 measured by EPMA.

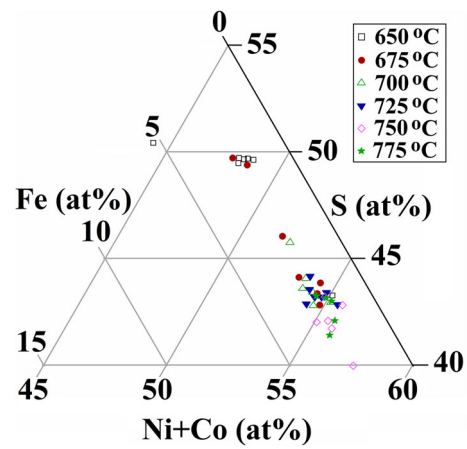


Fig. 9—Fe-(Ni + Co)-S ternary diagram shows the composition change of the pentlandite sulfide cores as a function of fluidized bed roasting temperatures by EPMA.

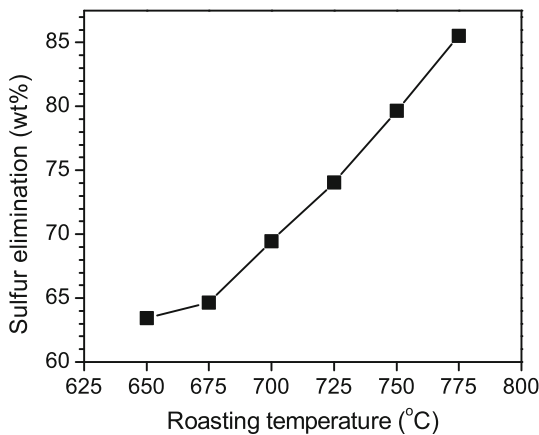


Fig. 8—Degree of sulfur elimination as a function of roasting temperature.

Figure 8 reveals the degree of sulfur elimination as a function of roasting temperature. Previous study by other researchers<sup>[22]</sup> shows that the roasting rate was limited by the mass transfer of O<sub>2</sub> to the reaction interface through the oxide rims that were formed upon oxidation. Considering this, the increase of sulfur elimination with the increasing roasting temperature is possibly caused by the acceleration of O<sub>2</sub> diffusion through the porous oxide layers at higher temperatures. Previous study<sup>[21]</sup> has shown that different sulfide species in the Ni concentrate were oxidized at various temperature ranges. Some sulfides were oxidized with a multi-step mechanism, which is also temperature dependent. This temperature dependency of oxidation roasting reactions could be another important factor that causes the dependency of the degree of sulfur elimination on temperature.

In order to further observe the roasting behavior of the nickel concentrate under different roasting temperatures, roasted pentlandite sulfide cores were analyzed by EPMA for their chemical compositions, which are

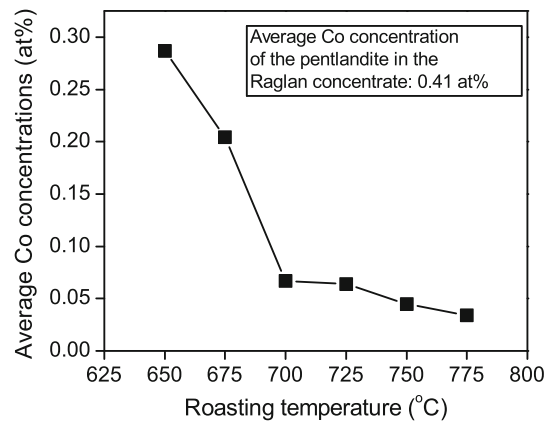


Fig. 10—Average Co concentrations of the roasted pentlandite sulfide cores as a function of the fluidized bed roasting temperatures by EPMA.

shown in Figures 9 and 10. Figure 9 illustrates the chemical composition change in a ternary Fe-(Ni + Co)-S diagram. As can be seen, Fe concentrations of most of the pentlandite derived particles are approximately 2 at pct, *i.e.*, they do not change with the increase of roasting temperatures. This value appears to represent the lowest iron concentration in the pentlandite by preferential oxidation. The Fe concentration reported in Figure 7 is approximately 6 at pct, which is much higher. This is because of its relatively large particle size ( $\sim 70 \mu\text{m}$ ) and the relatively low roasting temperature [923 K (650 °C)] employed. Our previous study<sup>[21]</sup> has shown that smaller pentlandite particles have higher preferential oxidation rate of Fe species, which is in good agreement with the results from this study. Sulfur concentration decreases from approximately 50 at pct to 44 at pct when temperature increases from 923 K to 973 K (650 °C to 700 °C) in Figure 9, with a corresponding increase in Ni contents from 48 at pct to 54 at pct. This change in sulfur contents coincides well with the disappearance of mss with the general formula (Fe,Ni)<sub>1-x</sub>S above 948 K (675 °C), which is illustrated in Figure 5 and

represented by Reaction [4]. Further temperature increase above 973 K (700 °C) does not contribute to an obvious change in composition.

During the oxidation roasting of the nickel concentrate, Co species were also partially oxidized and removed from the sulfide cores along with the oxidation of the Fe species. Figure 10 indicates the Co concentration of the roasted pentlandite sulfide cores as a function of roasting temperature. The average Co concentration in the pentlandite particles without roasting is 0.41 at pct. After roasting the concentrate at 923 K (650 °C), the Co concentration in the pentlandite sulfide cores dropped to 0.29 at pct. A substantial decrease in Co concentration in the roasted pentlandite particles can also be observed between 923 K and 973 K (650 °C and 700 °C). Above 973 K (700 °C), the Co concentration dropped at a much lower rate.

A roasting sequence of metal species in the pentlandite can thus be tentatively suggested as follows. Preferential oxidation starts with the oxidation of iron sulfide from the pentlandite ((Fe,Ni)<sub>9</sub>S<sub>8</sub>) forming Fe<sub>x</sub>Ni<sub>1-y</sub>S containing approximately 2 at pct Fe. Further roasting leads to the oxidation of nickel sulfide species toward Fe<sub>x</sub>Ni<sub>3-y</sub>S<sub>2</sub>, which is a more sulfur deficient phase. During the decrease in sulfur content, substantial percentages of Co in the pentlandite is oxidized and removed from the sulfide cores. For complete/dead roasting, the final oxidation should be the oxidation of the remaining nickel sulfide to form nickel oxide.

In the industrial oxidation roasting practice, the oxygen utilization efficiency is close to 100 pct. However, excessive amount of air was used for roasting in this study, resulting in high partial pressure of O<sub>2</sub> as well as SO<sub>2</sub> in the fluidized bed and in the offgas. This provides more favorable conditions for sulfates formation compared with the industrial roasting practice. In order to evaluate metal sulfate formation during oxidation roasting of this study, calcines were leached with hot water for 30 min to produce leachates for ICP analysis. Results are plotted in Figure 11 as percent extraction of elements from the calcines by water as a function of the roasting temperature calculated based on Eq. [1]. As can be seen, iron sulfate extraction is close to nil under these temperatures. Copper sulfate formation drops to close to zero at 948 K (675 °C). Nickel as sulfate stays at approximately 20 wt pct when temperature is below 973 K (700 °C), above which it drops substantially. Cobalt sulfate content drops continuously from 923 K to 1048 K (650 °C to 775 °C), but substantial drop occurs when the roasting temperature is above 973 K (700 °C). Magnesium sulfate content remains relatively constant, at around 27 wt pct. Soluble silicon content is constant as well, at around 5 wt pct of silicon in the feed. Smaller amounts of sulfates were formed at higher temperatures because oxides were preferentially formed rather than sulfates.

### B. Effect of Roasting Time

Another series of roasting experiments was performed at 1023 K (750 °C) to evaluate the effect the roasting time. Calcines were analyzed with XRD for their

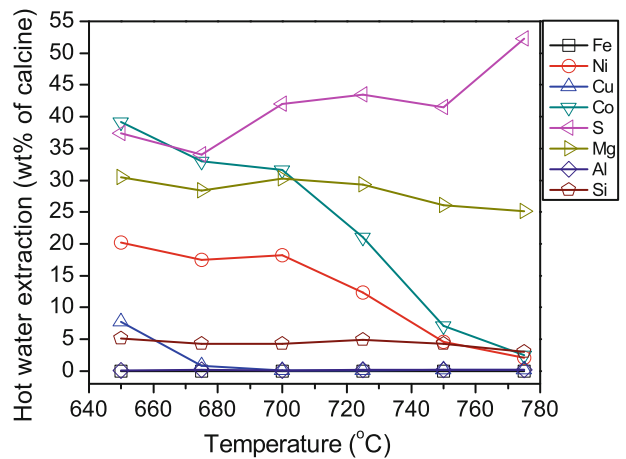


Fig. 11—Water-soluble species (wt pct) in the roasted calcines vs roasting temperature.

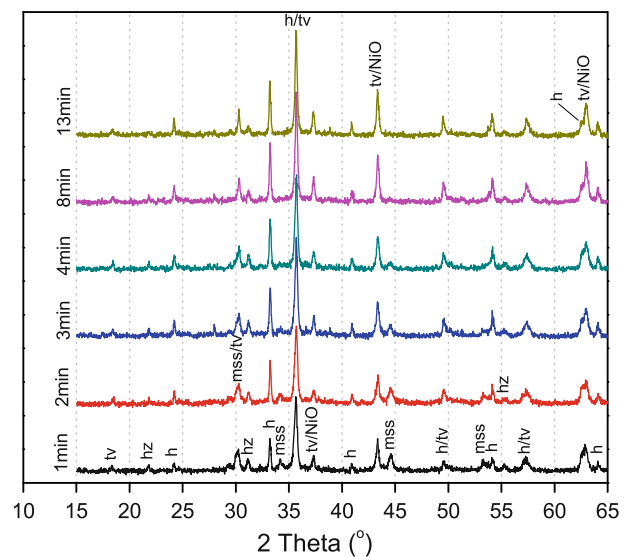


Fig. 12—XRD patterns for the fluidized bed roasting tests at 1023 K (750 °C) with roasting time variation (lv: trevorite, mss: monosulfide solid solution, h: hematite, NiO: nickel oxide, hz: heazlewoodite).

qualitative mineral compositions, and their XRD patterns are provided in Figure 12. As expected and can be seen from this figure, considerable roasting took place within 1 minute, resulting in the disappearance of all the original sulfide minerals and formation of various oxidized phases, *i.e.*, trevorite (NiFe<sub>2</sub>O<sub>4</sub>), hematite (Fe<sub>2</sub>O<sub>3</sub>), mss ((Fe,Ni)<sub>1-x</sub>S), NiO, and heazlewoodite (Ni<sub>3</sub>S<sub>2</sub>). The preferential oxidation of iron sulfide species forming iron oxides occurred within this first minute. Roasting reactions could be represented by Reactions [2] and [3]. Further roasting led to the disappearance of mss after 4 min (Reaction [4]), as well as the formation of more oxides, *i.e.*, hematite, trevorite, and NiO.

Figure 13 illustrates the degree of sulfur elimination as a function of roasting time at 1023 K (750 °C). Within 1 min the sulfur removal reached 63 pct, indicating a high roasting rate at the beginning. The

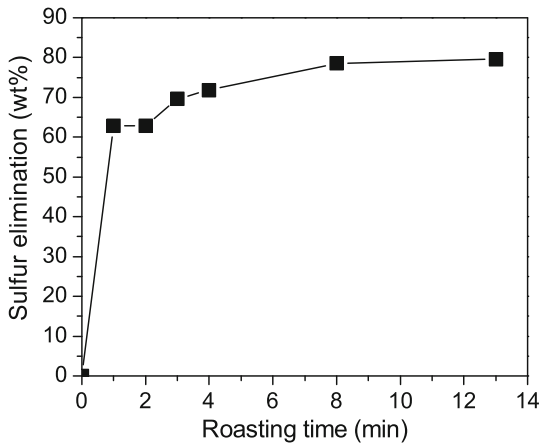


Fig. 13—Degree of sulfur elimination as a function of roasting time at 1023 K (750 °C).

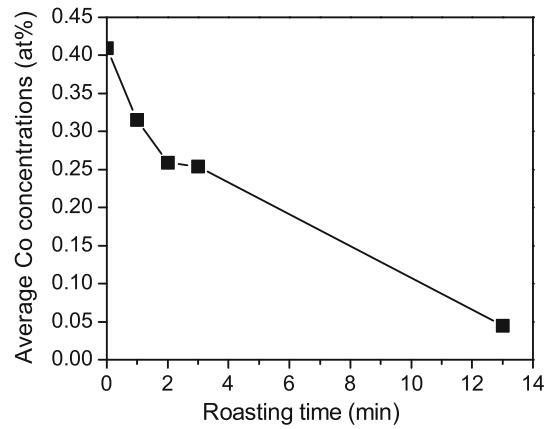


Fig. 15—Average Co concentrations of the roasted pentlandite sulfide cores as a function of the fluidized bed roasting time measured by EPMA.

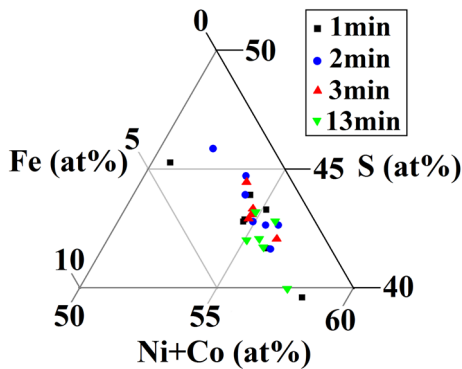


Fig. 14—Fe-(Ni + Co)-S ternary diagram shows the composition change of the pentlandite sulfide cores as a function of fluidized bed roasting time by EPMA.

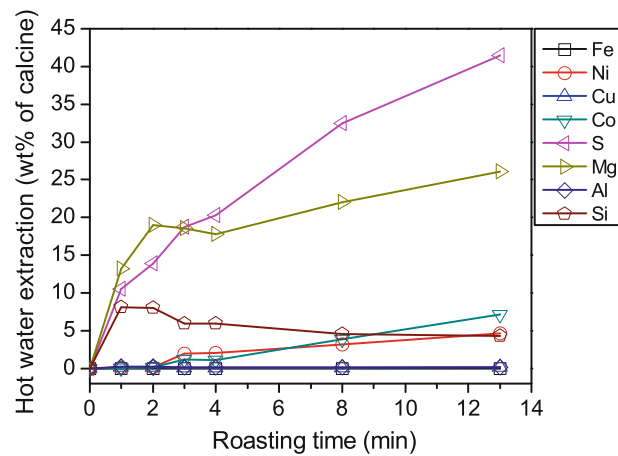


Fig. 16—Water-soluble species (wt pct) in the roasted calcines vs roasting time at 1023 K (750 °C).

rate of sulfur elimination is then decreased until it becomes practically zero after around 8 min, where the curve reaches a plateau at around 79 pct. The remaining 21 pct sulfur in the calcine is in the form of heazlewoodite base on the XRD analysis shown in Figure 12. Figure 14 shows the chemical composition change of the roasted pentlandite sulfide cores as a function of roasting time. As can be seen, the iron concentration in the pentlandite sulfide cores is reduced to the minimum 2 at pct after 1 min (Reaction [3]). Longer roasting time leads to the further oxidation of nickel sulfide (NiS) to form Ni<sub>3</sub>S<sub>2</sub> (Reaction [4]). In Figure 15, the average Co concentration of roasted pentlandite sulfide cores is plotted as a function of roasting time. As observed, the oxidation rate of cobalt from pentlandite is relatively high at the beginning of roasting then slows down as the roasting proceeds. The average Co concentration dropped to be approximately 0.05 pct after 13 min.

Calcines from these tests were also subject to water leaching and ICP analysis. The results are presented in Figure 16. An interesting observation is that within the first 2 min, only Mg and Si were dissolved among all the

metal elements. The formation of NiSO<sub>4</sub> started after 2 min. This is possibly because within the first 2 minutes iron from the pentlandite particles was preferentially oxidized, and the nickel sulfide would not likely be sulfated before the iron content in the pentlandite reaches its minimum, *i.e.*, 2 at pct. Figure 16 also illustrates that no sulfates of iron or copper were formed at the temperature as high as 1023 K (750 °C) under the current roasting conditions.

#### IV. CONCLUSIONS

A laboratory scale, batch fluidized bed roaster was constructed to study the oxidation roasting of a nickel sulfide concentrate. Roasting tests were carried out at temperatures between 923 K and 1048 K (650 °C and 775 °C). At all temperatures, oxidation roasting reactions mainly occurred within the first minute and usually lasted no longer than 10 min. Roasting reactions proceed as following: The reactions start with the



preferential oxidation of iron sulfide species forming iron oxides until the concentration of Fe in the pentlandite sulfide cores drops to 2 at pct. The remaining nickel sulfide core in the pentlandite particles is either NiS or Ni<sub>3</sub>S<sub>2</sub> depending on the roasting temperature, *i.e.*, the nickel sulfide formed tends to be more sulfur deficient at higher temperatures. The formation of sulfates of Ni and Co occurs after the oxidation of iron sulfide. Low temperature [*e.g.*, 923 K (650 °C)] is favorable for the preferential oxidation of iron sulfide species while minimizing the formation of nickeliferous oxides, *i.e.*, trevorite and NiO; the formation of these phases is inevitable for the roasting at temperatures higher than 973 K (700 °C) in air. In the range of 923 K to 1048 K (650 °C to 775 °C) no iron sulfate was formed. Higher degree of sulfur elimination could be achieved at higher temperatures. Sulfates formation was inhibited at higher temperatures at the cost of forming more oxides. Unlike the oxidation of iron sulfide, the oxidation of Co species is a slow process. The oxidation of the nickel sulfide core Ni<sub>3</sub>S<sub>2</sub> is the last step if the roasting temperature is high enough.

#### ACKNOWLEDGEMENTS

The authors thank Xstrata Process Support (Sudbury, Ontario, Canada) for providing the concentrate and both Xstrata and Vale for sponsoring the project. Special thanks are due to Yanan Liu of the Department of Geology of the University of Toronto for her assistance in the characterization of the samples. We would also like to express our sincere thanks to Dr. Gus Van Weert of the ORETOME Ltd. for his constructive comments on this paper. The funding for this research was provided by the Natural Sciences and Engineering Research Council (NSERC) of Canada.

#### REFERENCES

1. B. Terry, A.J. Monhemius, and A.R. Burkin: *Extractive Metallurgy of Nickel*, Wiley, New York, 1987, pp. 1–6.
2. A.E.M. Warner, C.M. Diaz, A.D. Dalvi, P.J. Mackey, and A.V. Tarasov: *J. Met.*, 2006, vol. 58, pp. 11–20.
3. F.K. Crundwell, M.S. Moats, V. Ramachandran, T.G. Robinson, and W.G. Davenport: *Extractive Metallurgy of Nickel, Cobalt and Platinum-Group Metals*, Elsevier, Oxford, 2011, pp. 117–122.
4. A.E.M. Warner, C.M. Diaz, A.D. Dalvi, P.J. Mackey, A.V. Tarasov, and R.T. Jones: *J. Met.*, 2007, vol. 59, pp. 58–72.
5. F.K. Crundwell, M.S. Moats, V. Ramachandran, T.G. Robinson, and W.G. Davenport: *Extractive Metallurgy of Nickel, Cobalt and Platinum-Group Metals*, Elsevier, Oxford, 2011, pp. 21–37.
6. F.K. Crundwell, M.S. Moats, V. Ramachandran, T.G. Robinson, and W.G. Davenport: *Extractive Metallurgy of Nickel, Cobalt and Platinum-Group Metals*, Elsevier, Oxford, 2011, pp. 247–57.
7. J.R. Boldt, Jr.: *The Winning of Nickel*, Longmans Canada, Toronto, 1967, pp. 331–36.
8. A.W. Fletcher and K.D. Hester: *AIME Trans.*, September 1964, pp. 282–91.
9. A.W. Fletcher and M. Shelef: *Trans. TMS-AIME*, 1964, vol. 230, pp. 1721–24.
10. A.W. Fletcher and M. Shelef: *Unit Process in Hydrometallurgy. Group C: Plant Operating Practice—Economics—General*, Gordon and Breach Science Publishers, New York, 1965, pp. 946–70.
11. T.C. Frankiewicz: U.S. Patent 4,110,106, 29 August 1978.
12. M.C.B. Hotz, R.C. Kerby, and T.R. Ingraham: *Can. Metall. Q.*, 1968, vol. 7, pp. 205–210.
13. P.J. Saikkonen: U.S. Patent 4,464,344, 7 Aug 1984.
14. P.J. Saikkonen and J.K. Rastas: Paper presented at the 25th Annual Conference of Metallurgists, Toronto, Ontario, Canada, 1986, pp. 278–90.
15. P.G. Thornhill: U.S. Patent 2,813,015, 12 Nov 1957.
16. P.G. Thornhill: U.S. Patent 2,813,016, 12 Nov 1957.
17. D. Yu, M. Zhu, T.A. Utigard, and M. Barati, *Miner. Eng.*, 2013, <http://dx.doi.org/10.1016/j.mineng.2013.03.018>.
18. D. Yu, T.A. Utigard, and M. Barati: *Metall. Mater. Trans. B*, 2013, DOI:10.1007/s11663-013-9959-9.
19. H.Y. Sohn and R.P. Goel: *Miner. Sci. Eng.*, 1979, vol. 11, pp. 137–53.
20. D. Geldart: *Powder Technol.*, 1973, vol. 7, pp. 285–92.
21. D. Yu and T.A. Utigard: *Thermochim. Acta*, 2012, vol. 533, pp. 56–65.
22. M. Zamalloa and T.A. Utigard: *Can. Metall. Q.*, 1996, vol. 35, pp. 435–49.